



HAL
open science

Electrostatic Potential Radiated by a Pulsating Charge in a Two-Electron Temperature Plasma

Nicolas Gilet, Pierre Henri, Gaëtan Wattieaux, Marco Cilibrasi, Christian Béghin

► **To cite this version:**

Nicolas Gilet, Pierre Henri, Gaëtan Wattieaux, Marco Cilibrasi, Christian Béghin. Electrostatic Potential Radiated by a Pulsating Charge in a Two-Electron Temperature Plasma. *Radio Science*, 2017, 52 (11), pp.1432-1448. 10.1002/2017RS006294 . insu-01666682

HAL Id: insu-01666682

<https://insu.hal.science/insu-01666682>

Submitted on 19 Dec 2017

HAL is a multi-disciplinary open access archive for the deposit and dissemination of scientific research documents, whether they are published or not. The documents may come from teaching and research institutions in France or abroad, or from public or private research centers.

L'archive ouverte pluridisciplinaire **HAL**, est destinée au dépôt et à la diffusion de documents scientifiques de niveau recherche, publiés ou non, émanant des établissements d'enseignement et de recherche français ou étrangers, des laboratoires publics ou privés.



RESEARCH ARTICLE

10.1002/2017RS006294

Electrostatic Potential Radiated by a Pulsating Charge in a Two-Electron Temperature Plasma

N. Gilet¹, P. Henri¹ , G. Wattieaux², M. Cilibrasi^{1,3,4} , and C. Béghin¹ ¹LPC2E, CNRS, Université d'Orléans, Orléans, France, ²Université de Toulouse, Toulouse, France, ³Scuola Normale Superiore, Pisa, Italy, ⁴Dipartimento di Fisica "Enrico Fermi", Università di Pisa, Pisa, Italy

Key Points:

- The potential radiated by a pulsating point charge has been computed by a numerical integration
- Mutual impedance spectra are predicted in a two-electron temperature plasma; the influence of the temperature ratio is discussed
- Two resonances are identified at the total and cold plasma frequencies, from which the cold/hot densities can be extracted

Correspondence to:

N. Gilet,
nicolas.gilet@cns-orleans.fr

Citation:

Gilet, N., Henri, P., Wattieaux, G., Cilibrasi, M., & Béghin, C. (2017). Electrostatic potential radiated by a pulsating charge in a two-electron temperature plasma. *Radio Science*, 52. <https://doi.org/10.1002/2017RS006294>

Received 7 MAR 2017

Accepted 1 OCT 2017

Accepted article online 31 OCT 2017

Abstract Mutual impedance experiments have been developed to constrain the plasma bulk properties, such as density and temperature, of ionospheric and later space plasmas, through the electric coupling between an emitter and a receiver electric antennas. So far, the analytical modeling of such instruments has enabled to treat ionospheric plasmas, where charged particles are usually well characterized by Maxwellian electron distributions. With the growth of planetary exploration, mutual impedance experiments are or will be used to constrain space plasma bulk properties. Space plasmas are usually out of local thermodynamic equilibrium; therefore, new methods to calibrate and analyze mutual impedance experiments are now required in such non-Maxwellian plasmas. To this purpose, this work aims at modeling the electric potential generated in a two-electron temperature plasma by a pulsating point charge. A numerical method is developed for the computation of the electrostatic potential in a sum of Maxwellian plasmas. After validating the method, the results are used to build synthetic mutual impedance spectra and quantify the effect of a warm electron population on mutual impedance experiments, in order to illustrate how the method could be applied for recent and future planetary space missions, such as Rosetta, BepiColombo, and JUICE. In particular, we show how it enables to separate the densities and temperatures of two different electron populations using in situ measurements from the RPC-MIP mutual impedance experiment on board Rosetta.

1. Introduction

Mutual impedance probe experiments have been used in various ionized environments, from ionospheric to interplanetary plasmas, to constrain plasma parameters such as the electron density, the electron temperature, and the plasma drift velocity. From the 1970s, such experiments have been launched on the ionospheric rocket CISASPE (Béghin & Debrie, 1972), as well as satellites such as Geostationary Earth Orbit Satellite 1 (or GEOS-1) (Décréau et al., 1978), ARCAD-3 (Béghin et al., 1982), VIKING (Bahnsen et al., 1986), Rosetta (Trotignon et al., 2007), and are planned for future space missions: BepiColombo (Trotignon et al., 2006) and JUICE. These experiments included an active electrical probe usually made of two receiving and two transmitting electric antennas. The probe operates close to the typical plasma frequencies which are typically found in the radio frequency (RF) range in space plasma environments. A RF electric field is induced in the probed medium through the transmitters with the help of a frequency adjustable current generator. Then the induced voltage (amplitude and phase) between the receivers is recorded as a function of the frequency. The voltage acquired in the plasma is divided by the voltage acquired in vacuum to provide the so-called response of the probe. More information about mutual impedance probes can be found in Storey et al. (1969) and Storey (1998).

Plasma properties are determined from the response of the probe. In the following, we focus on the frequency range close to the plasma frequency which enables to constrain the plasma density. The instrumental response strongly depends on the electron velocity distribution function (evdf). Many theoretical works have been published for the past five decades (Béghin, 1995; Grard, 1969; Navet et al., 1971; Pottellette et al., 1975; Rooy et al., 1972), using different analytical approximations of the plasma dielectric function corresponding to different plasma conditions, from the cold case to a hot plasma with different velocity distributions, some of which are summarized in Chasseriaux et al. (1972). Both the collisional and collisionless cases have been investigated. To better take into account the behavior of a thermal plasma on mutual impedance experiments, including the Landau damping of the waves emitted by the transmitters, Béghin (1995) determined the

analytical solution of the potential radiated by a point source in a collisionless Maxwellian plasma, using a series expansion of the dielectric function.

Such approximations are consistent in ionospheric plasmas. However, interplanetary plasmas are usually collisionless and therefore are characterized by non thermalized velocity distribution functions. In particular, suprathermal electrons have been commonly observed in space plasmas, superposed to a Maxwellian-like core (Pilipp et al., 1987). Such evdf are usually described by the superposition of two Maxwellian evdf, or by a kappa function (Pierrard & Lazar, 2010).

Previous authors investigated the influence of suprathermal electrons on active experiments such as mutual impedance probes. These previous approaches had the advantage to enable analytic computations of the potential radiated in a plasma in specific plasma or geometric situations that are tractable analytically.

Grard (1997) investigated the influence of suprathermal electrons on mutual impedance probes by considering monoenergetic electron distribution functions. However, this approach does not include the influence of thermal effects, such as Landau damping, on the propagation of the electric potential from the emitting to the receiving antenna, which are known to strongly impact the mutual impedance spectra at frequencies above the plasma frequency. In this work, we aim at developing a method that will allow to account for the collisionless Landau damping of the potential radiated by the emitting antennas of mutual impedance experiments.

Pottelette and Storey (1981) approximated the influence of two populations with Maxwellian distribution using specific values for the temperature ratio and the hot-to-cold population density ratio. However, the analytic dipole approximation used in this approach is valid in the limit of (i) an emitter-receiver distance l much larger than the emitter-emitter and receiver-receiver distances and (ii) an emitter-receiver distance much larger than the hot and cold Debye lengths. While such a configuration can be of strong interest in ionospheric plasmas (where the Debye length is much smaller than the experiment size), interplanetary plasmas are often characterized by a Debye length that is not much larger than typical electric antennas, but rather of similar size: in the solar wind, the Debye length is about 20 m at 1 AU, while it has been evaluated to be in the 30 cm to 1 m range for the cometary ionosphere probed by Rosetta (Odelstad et al., 2015). Moreover, active electric antennas on board interplanetary spacecraft such as Rosetta, BepiColombo, and JUICE are designed such that the emitter-receiver distances are of the order of the emitter-emitter and receiver-receiver distances, in the 1–20 m range. It is therefore necessary to develop a method that also enables to model the radiated electric potential at short distances from the emitter, at least at distances of the order of the Debye length itself, as addressed in this work.

This study also intends to extend the work done for a collisionless Maxwellian plasma in Beghin (1995) to a plasma composed of two-electron populations, modeled as the superposition of two isotropic Maxwellian evdf. The series development proposed in Beghin (1995) for a Maxwellian evdf would be particularly tedious in the case of a sum of two Maxwellian evdf. This is the reason why we decided to use a direct numerical integration of the potential radiated by a point source. We first validate the computation method by comparing the numerical results to the analytical ones in the cases of a cold and a Maxwellian evdf plasma. Then, we study a sum of two Maxwellian isotropic collisionless plasmas situation. We focus our study on the unmagnetized plasma limit, that is, to plasmas where the electron plasma frequency is much larger than the electron cyclotron frequency. In the electrostatic regime close to the electron plasma frequency, both the ion dynamics and the influence of the magnetic field can be neglected. We hereafter consider a fixed background of ions, together with global neutrality. The plasma electrostatic sheath surrounding the probe immersed in the plasma is neglected in this work. Its contribution to the response of the probe, necessary to properly model mutual impedance probe data, will be studied in a future publication.

This paper is organized as follows. The theoretical expression of the potential induced by a pulsating point charge in an isotropic plasma is recalled in section 2 for different evdf of interest. In section 3, the numerical method used to compute the radiated electric potential in a plasma is presented and validated. In section 4, we discuss the ideal response of a mutual impedance probe immersed in a sum of two Maxwellian evdf plasma and compare it to a single-electron population plasma. Finally, the method is applied on a data set from the Rosetta mutual impedance experiment RPC-MIP in section 5.3 to illustrate how the density and temperature of the two different electron populations can be extracted. We conclude our study in section 6.

2. Potential Induced by a Pulsating Point Charge in an Isotropic Plasma

The potential ϕ induced in an isotropic, homogeneous plasma by a pulsating point charge $Q \cdot \exp(i\omega t)$, at frequency ω , at a radial distance r from the charge (Chasseriaux et al., 1972) is given by

$$\phi(\omega, r) = \frac{Q}{4\pi\epsilon_0} \frac{2}{\pi} \lim_{\text{Im}(\omega) \rightarrow 0} \int_0^\infty \frac{\sin(kr)}{kr} \frac{dk}{\epsilon_l(k, \omega)} \quad (1)$$

with ϵ_l the longitudinal dielectric function of the plasma, k the wave vector, and ϵ_0 the vacuum permittivity (see Beghin (1995), and reference therein, for more details).

In this section, we remind the expression of the longitudinal dielectric function in the cases of a cold and a sum of Maxwellian plasmas, respectively, and we introduce the notations used in the rest of the work.

2.1. Cold Plasma

The cold plasma is the limit case of a Maxwellian plasma with an electron temperature $T_e=0$. The dielectric function in a cold collisionless plasma is given by

$$\epsilon_l^{\text{cold}}(\omega) = 1 - \left(\frac{\omega_p}{\omega}\right)^2 \quad (2)$$

where the electron plasma frequency ω_p is defined by

$$\omega_p = \sqrt{\frac{n_e e^2}{\epsilon_0 m_e}} \quad (3)$$

with the electron density n_e , the elementary charge e , the electron mass m_e , and the vacuum permittivity ϵ_0 . The dielectric function ϵ_l does not depend on the wave vector k in the cold plasma limit.

Using equation (1), the potential ϕ induced in a cold, collisionless plasma by a pulsating point charge $Q(\omega)$ at frequency ω finally reads

$$\phi(\omega, r) = \frac{Q}{4\pi\epsilon_0 r} \frac{\omega^2}{\omega^2 - \omega_p^2} \quad (4)$$

while $\phi_0 = Q / (4\pi\epsilon_0 r)$ is the potential induced by the pulsating point charge at a radial distance r in free space. Finally, the potential induced in a cold plasma, normalized to the potential induced in vacuum, reads

$$\frac{\phi}{\phi_0}(\omega) = \frac{\omega^2}{\omega^2 - \omega_p^2} \quad (5)$$

2.2. A Sum of Maxwellian Plasma

A sum of m Maxwellian evdf is characterized by electron density n_i and the temperature T_i of each population. These parameters provide the electron thermal velocity $v_{\text{th},i}$ and the Debye length $\lambda_{D,i}$:

$$v_{\text{th},i} = \sqrt{\frac{k_B T_i}{m_e}} \quad (6)$$

$$\lambda_{D,i} = \sqrt{\frac{\epsilon_0 k_B T_i}{n_i e^2}} \quad (7)$$

with k_B the Boltzmann constant. We hereafter define the plasma frequencies $\omega_{p,i}^2 = \frac{n_i e^2}{\epsilon_0 m_e}$, so that the (total) plasma frequency reads $\omega_p^2 = \sum_{i=1}^m \omega_{p,i}^2$. Moreover, we will make use of the ratios of density (resp. temperature) with the first population $\mu_i = \frac{N_i}{N_1}$ (resp. $\tau_i = \frac{T_i}{T_1}$) where N_j is the density n_j normalized by the total density. For a collisionless isotropic plasma with a sum of Maxwellian evdf, the dielectric function is given by

$$\epsilon_l^m(K, \Omega) = 1 - \sum_{i=1}^m \frac{Y_i^2}{\Omega_i^2} Z'(Y_i) \quad (8)$$

where

$$K = k\lambda_{D,1} \quad (9)$$

$$\Omega_i = \frac{\omega}{\omega_{p,i}} \quad (10)$$

$$\lambda_{D,i} = \sqrt{\frac{\mu_i}{\tau_i}} \lambda_{D,1} \quad (11)$$

$$Y_i = \frac{\Omega_i}{\sqrt{2\mu_i/\tau_i}K} \quad (12)$$

and Z' is the first derivative of the plasma dispersion function Z (Fried & Conte, 1961). This function satisfies the differential equation $Z'(y) = -2(1 + y \cdot Z(y))$ and derived from the Faddeeva function w (or the scaled complex complementary error function):

$$Z(y) = i\sqrt{\pi}w(y) \quad (13)$$

defined by

$$w(y) = \exp(-y^2) \left(1 + \frac{2i}{\sqrt{\pi}} \int_0^y \exp(-t^2) dt \right) \quad (14)$$

Normalizing the distance to the point source using the Debye length of the first population $R = \frac{r}{\lambda_{D,1}}$, the electric potential reads

$$\frac{\phi}{\phi_0}(\Omega, R) = \frac{2R}{\pi} \lim_{\text{Im}(\Omega) \rightarrow 0} \int_0^{\infty} \frac{\sin(KR)}{KR} \frac{1}{\epsilon_l^m(K, \Omega)} dK \quad (15)$$

In this study, we focus on a Maxwellian plasma ($m = 1$) and a two-temperature plasma ($m = 2$). For a Maxwellian plasma, $\lambda_{D,1}$ is noted λ_D . For $m = 2$, the evdf is characterized by four parameters: $n_1 = n_h$, $n_2 = n_c$, $T_1 = T_h$, and $T_2 = T_c$ which are, respectively, the electron density of the hottest electron population and the electron density of the coldest one their corresponding electron temperatures.

The potential induced by a pulsating charge in a plasma (equation (15)) is required to compute the response of a mutual impedance probe, as shown in the next section.

2.3. Response of a Mutual Impedance Probe

We hereafter consider a mutual impedance probe, composed of two electric monopole antenna receivers and different electric emitters. The emitters inject a constant current I , acting as pulsating point charges, at a given frequency ω , while the receivers measure the (complex) amplitude of the electric potential at the same frequency. A mutual impedance spectrum is build by varying, step by step, the emitted frequency. The mutual impedance $Z(\omega) = \Delta V(\omega)/I$ is then defined as the difference between the electric potential $\Delta V(\omega) = V_{R_2}(\omega) - V_{R_1}(\omega)$, radiated by the different emitters at frequency ω and measured by two receivers R_1 and R_2 at this same frequency. To isolated the effect of the plasma on the potential radiated by the emission part of a mutual impedance probe, we work with the mutual impedance spectrum normalized to the spectrum that is obtained in vacuum

$$H(\omega) = \frac{\Delta Z}{\Delta Z_0} = \frac{V_{R_2}(\omega) - V_{R_1}(\omega)}{V_{R_2,0} - V_{R_1,0}} \quad (16)$$

where ΔZ and ΔZ_0 represent the mutual impedance of a probe surrounded by a plasma and by the vacuum, respectively, and V_{R_i} (resp. $V_{R_i,0}$) is the voltage measured by the receiver R_i in the plasma (resp. in vacuum) which are defined as follows:

$$V_{R_i,0} = \frac{1}{4\pi\epsilon_0} \sum_{j=1}^N \frac{q_j}{d_{ij}} \quad (17)$$

$$V_{R_i}(\omega) = \frac{1}{4\pi\epsilon_0} \sum_{j=1}^N \frac{\phi}{\phi_0}(\Omega, d_{ij}/\lambda_{D,1}) \frac{q_j}{d_{ij}} \quad (18)$$

where q_j is the charge of the j th emitter and d_{ij} is the distance between the receiver R_i and the j th emitter. In this study, the mutual impedance probe is considered at electric charge equilibrium, that is, $\sum q_j = 0$. $H(\omega)$ is called response in the rest of the paper.

2.4. Linear Eigenmodes

In this section, we remind the analytic approximations of the linear eigenmodes of cold, Maxwellian and two Maxwellian electrostatic plasmas. They enable a simplified interpretation of the propagation of the electric potential in a plasma and also enable to quickly locate the resonances that are observed in mutual impedance spectra.

They can be found in classic plasma textbooks as poles of the dielectric function, computed in specific regimes that are tractable analytically. The numerical integration described in the next section will allow to compute the radiated potential without working in the range of parameters for which these analytic approximations are derived. However we choose in this section to discuss those approximated electrostatic linear eigenmodes in order to enable physical insight into the results presented in the rest of the paper.

1. In the cold plasma case, the dielectric is such that the only eigenmode mode is found at the plasma frequency.
2. In the Maxwellian plasma case, at high enough frequencies, such that the ions can be considered at rest, the least damped poles of the dielectric function are the Langmuir waves characterized in the large phase velocity limit $\omega/k \gg v_{th}$ by the dispersion relation (Krall & Trivelpiece, 1973):

$$\omega_L(k) = \omega_p \sqrt{1 + 3(k\lambda_D)^2} - i\sqrt{\frac{\pi}{8}} \frac{\omega_p}{(k\lambda_D)^3} e^{-\frac{1}{2(k\lambda_D)^2} - \frac{3}{2}} \quad (19)$$

3. In a plasma characterized by a sum of two Maxwellian evdf, the Langmuir branch is modified in a way such that the thermal correction is mainly influenced by the hot electron component (through the total electron pressure, which is roughly the hot electron pressure), while the waves oscillate at the (total) plasma frequency. With v_h (resp. v_c) the thermal velocity of the hot (resp. cold) electron population and n_h (resp. n_{tot}) the hot (resp. total) electron density, the associated complex frequency ω_{L2} can be expressed in the limit $\frac{\omega}{k} \gg v_h \gg v_c$, (Buti & Yu, 1981), as

$$\omega_{L2}(k) = \omega_p \sqrt{1 + 3 \left(\frac{n_h}{n_{tot}} \right)^2 (k\lambda_{D,h})^2} - i\sqrt{\frac{\pi}{8}} \frac{\omega_p}{(k\lambda_{D,h})^3} e^{-\frac{1}{2(k\lambda_{D,h})^2}} \quad (20)$$

Moreover, a two-electron temperature plasma is characterized by the existence of another electrostatic mode: the electron acoustic wave. In the limit $v_c \ll \frac{\omega}{k} \ll v_h$ (Gary, 1993), the electron acoustic mode is characterized by the following dispersion relation:

$$\omega_{EAW}(k) = \omega_{p,c} \sqrt{1 + 3k^2 \lambda_{D,c}^2 - \frac{1}{k^2 \lambda_{D,h}^2}} - i\sqrt{\frac{\pi}{8}} \frac{\omega_{p,c}}{(k\lambda_{D,h})^3} \quad (21)$$

In a two-electron fluid approximation and in the limit of an intermediate phase velocity $v_c \ll \frac{\omega}{k} \ll v_h$, the electron acoustic mode is such that the plasma essentially oscillates with the inertia of the cold electron population ($\omega_{p,c}$ term), under the effect of the restoring electric and the pressure gradient forces, where the total pressure is dominated by the hot electron pressure. In the case of similar cold and hot electron pressure, the electron acoustic mode would be heavily Landau damped (as shown by a kinetic treatment) and would not propagate in the plasma anymore. Note that the electron acoustic mode in a two-electron population plasma is somehow equivalent to the ion acoustic mode in an ion-electron plasma, for which the ions oscillate under their own inertia and the effect of the restoring electric and the pressure gradient forces, where the pressure is essentially the electron pressure to avoid a strong Landau damping of the ion acoustic mode.

These modes structure the electric potential radiated in an unmagnetized plasma characterized by a single Maxwellian evdf and a sum of two Maxwellian evdf. In particular, they determine the resonances that shape the mutual impedance spectra. These analytic approximations are used, in the numerical computation of the radiated potential described in the next section, to identify the location of the poles of the dielectric function in K -space.

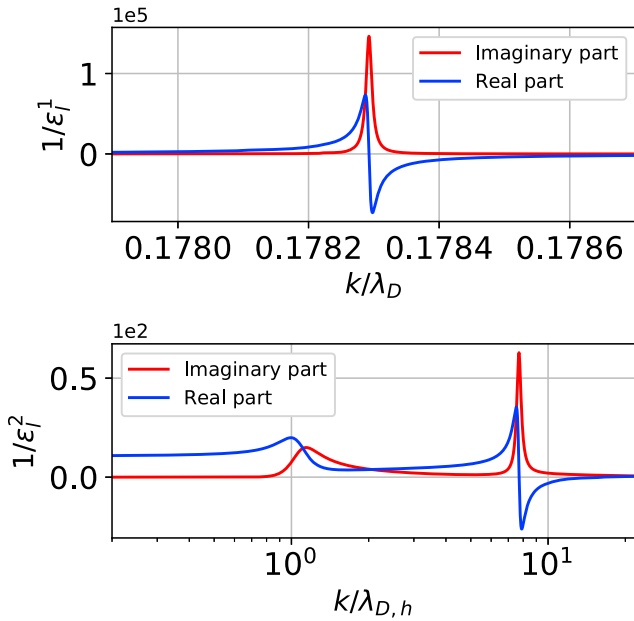


Figure 1. Real and imaginary parts of the (top) inverse of the dielectric function on the Maxwellian limit for $\Omega=1.05$ and a (bottom) sum of two Maxwellian evdf for $\Omega=1.05$, $\mu=0.11$, and $\tau=100$ with a zoom on the neighborhood of the poles.

3. Computation of the Potential

This section describes the highlights of computation of the radiated potential, using the dielectric constant for both a Maxwellian and a sum of two Maxwellian plasmas (section 3.1). On the Maxwellian limit, the numerical method extends the approaches developed for previous mutual impedance experiments (Beghin, 1995, and references therein). Written as an integral, the radiated potential equation (15) is computed using a numerical integration. The algorithm is validated in section 3.2.

3.1. Methodology

To compute numerically the radiated potential, the integral in equation (15) is split as follows:

$$\int_0^{+\infty} \frac{1}{\epsilon_i(\Omega, K)} \frac{\sin(KR)}{KR} dK = \underbrace{\int_0^{k_{\min}} \frac{1}{\epsilon_i(\Omega, K)} \frac{\sin(KR)}{KR} dK}_{I_1} + \underbrace{\int_{k_{\min}}^{k_{\max}} \frac{1}{\epsilon_i(\Omega, K)} \frac{\sin(KR)}{KR} dK}_{I_2} + \underbrace{\int_{k_{\max}}^{+\infty} \frac{1}{\epsilon_i(\Omega, k)} \frac{\sin(KR)}{KR} dK}_{I_3} \quad (22)$$

Integral I_1 is evaluated analytically, under some conditions regarding the choice of k_{\min} , and integral I_3 is shown to be negligible under some conditions regarding the choice of k_{\max} (Appendix A).

To evaluate I_2 with a numerical integration, the dielectric and the sinc functions are calculated on an initial K -space discretization, constrained by the conditions imposed on I_1 and I_3 (Appendix A).

The path of the numerical integration follows $\text{Im}(K) = 0$ so that K is a real number. However, in the complex K plane, the weakly damped poles K_i of the dielectric function are located close to the path of integration. In such cases, a specific numerical treatment is required to capture the strong variations of $1/\epsilon_i^1$, close to the singularity associated to the Langmuir eigenmode described in section 2.4. The shape of these strong variations, which occurs for frequency ω close to the plasma frequency ω_p , is illustrated in Figure 1 (top). In order to accurately integrate numerically I_2 , it is compulsory to carefully discretize $1/\epsilon_i^1$ in the close vicinity of the pole, where the discrete K -space is refined as described in Appendix A.

For a sum of two Maxwellian evdf, the computation of the dielectric function is done in a similar way. A main difference with the single Maxwellian case is the presence of another pole, associated to the electron acoustic mode discussed in section 2.4, close enough to the integration path (along the real K axis) for certain values of the parameters μ and τ to strongly influence the dielectric function. This is illustrated with the variation of $1/\epsilon_i^2$ in Figure 1 (bottom), for both its real and imaginary parts, which shows the influence on the integration path of the electron acoustic and the (modified) Langmuir poles. In general, the electron acoustic complex pole is sufficiently far away from the real axis (path of integration), so that grid refinements are only required in the close vicinity of the (modified) Langmuir pole.

3.2. Validation

In this section, we validate the numerical method described above, in the Maxwellian and a sum of two Maxwellian cases.

3.2.1. Validation of the Computation for a Maxwellian EVDF

To validate our numerical computation for a Maxwellian evdf, (i) we use the known asymptotic limits of the normalized electric potential ϕ/ϕ_0 and (ii) we also compare the mutual impedance obtained from our numerical computation to the one obtained in Beghin (1995) using a series expansion of the radiated electric potential.

1. As described in Beghin (1995), the real part of ϕ/ϕ_0 tends to the inverse of the cold plasma dielectric constant ϵ_c , given by $\epsilon_c = \frac{1}{1-\Omega^2}$, while the imaginary part tends to 0. This is illustrated in Figure 2, showing these asymptotic limits for $\Omega=0.90$ ($\epsilon_c^{-1} = -4.26$) and $\Omega = 1.50$ ($\epsilon_c^{-1} = 1.80$).

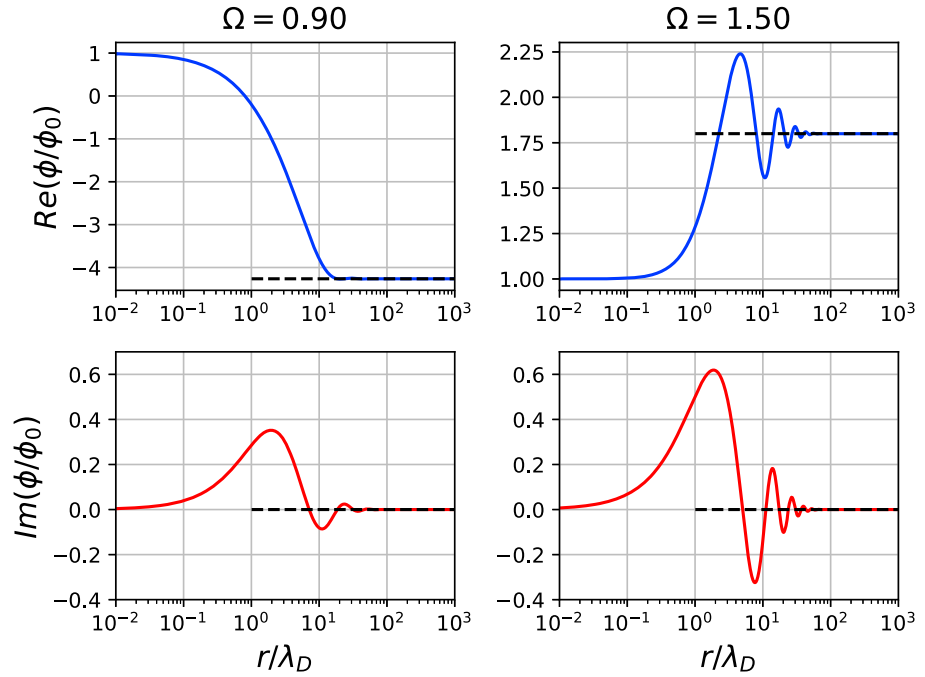


Figure 2. Real and imaginary parts of ϕ/ϕ_0 on the Maxwellian limit, for (left column) $\Omega = 0.9$ and (right column) $\Omega = 1.5$ with analytical limits (dashed lines).

2. In order to evaluate the impact of the evdf on the response of a mutual impedance probe, an idealized quadrupolar mutual impedance probe is considered, which geometry is shown in Figure 3, identical to the one chosen in Beghin (1995). It is composed of two oscillating point charges used as emitters (Q^+ and Q^-) and two potential receivers (R1 and R2). By considering $q_1 = -q_2$, we have computed $H(\Omega)$ in the above described geometry, for $\lambda_D = 0.1$ m. The corresponding spectra, obtained from our numerical integration, are shown in Figure 4. They are identical, both in amplitude and phase, to those obtained in Beghin (1995, Figure 10), where the dielectric function for Maxwellian evdf was approximated by a series expansion.

3.2.2. Validation of the Computation for a Two Maxwellian EVDF

The numerical computation for a two Maxwellian evdf has been validated as follows:

1. The cases $\tau = 1$, whatever the choice of μ , all reduce to the Maxwellian case. We check both that the positions of the Langmuir pole are identical and that the computation of the radiated potential of a point source ϕ/ϕ_0 is identical to the one obtained from the computation obtained from Maxwellian evdf. This is shown in Figure 5 (top), where the real positions of the Langmuir pole from a sum of two Maxwellian evdf case (black squares) are the same as with the computation done in the Maxwellian case (blue circles). Both are shown to asymptotically tend toward the long-wavelength analytical approximation from the Langmuir dispersion relation equation (19) (red line), that is, for a wave frequency close to the plasma frequency. Note that the distances are normalized to the Debye length λ_D in the Maxwellian case, while they are normalized to the Debye length of the hot population $\lambda_{D,h}$ in the two Maxwellian case.

2. We also validate the numerical computation in the case of a sum of two Maxwellian evdf, by comparing the position of the electron acoustic pole obtained numerically to the analytical approximation Ω_{EA0} in the limit $\mu \ll \tau$ (Gary, 1993), that is given from equation (21):

$$\Omega_{EA0}^2 = \Omega_c^2 \left(1 + 3K^2 \frac{\mu}{\tau} - \frac{1}{K^2} \right) \quad (23)$$

The validation is shown in Figure 5 (bottom), where the position of the electron acoustic pole from the numerical computation (black squares) tends toward the expected analytical approximation (red line) when Ω tends toward 0.

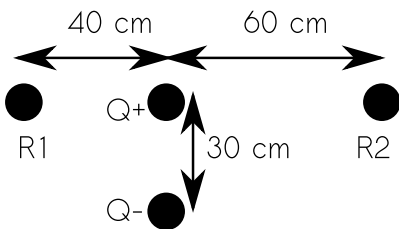


Figure 3. Example of quadrupolar mutual impedance probe made from two conducting spheres and two potential sensors, identical to the one described in Beghin (1995).

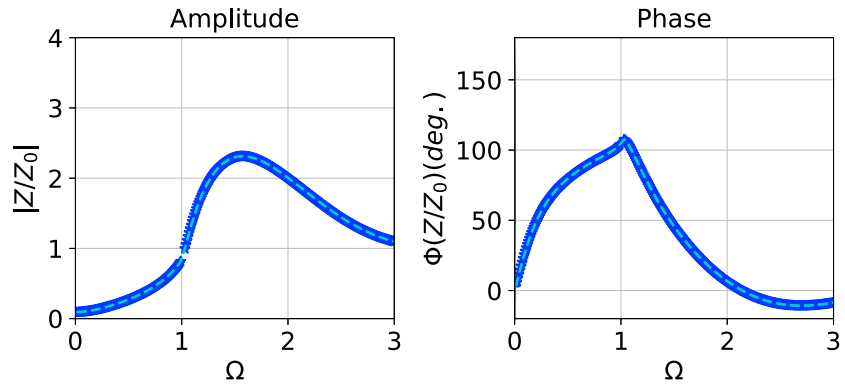


Figure 4. (left) Normalized response in modulus and (right) normalized response in phase for $\lambda_D = 0.1$ m on the idealized mutual impedance probe geometry (Figure 3) considered by Beghin (1995).

In a two-electron temperature plasma, the spatial variation of the electric potential radiated by a pulsating point charge is shaped, in a first approximation, by the superposition of the waves described in section 2.4. This is illustrated in Figure 6, for the potential computed at $\Omega = 1.10$ where both the electron acoustic and the (modified) Langmuir modes coexist with different wavelengths. The Langmuir wavelength is larger than the electron acoustic wavelength in this case, and the radiated electric potential appears as a short-wavelength oscillation (associated to a radiated electron acoustic wave), modulated by a longer-wavelength oscillation (associated to a radiated Langmuir wave).

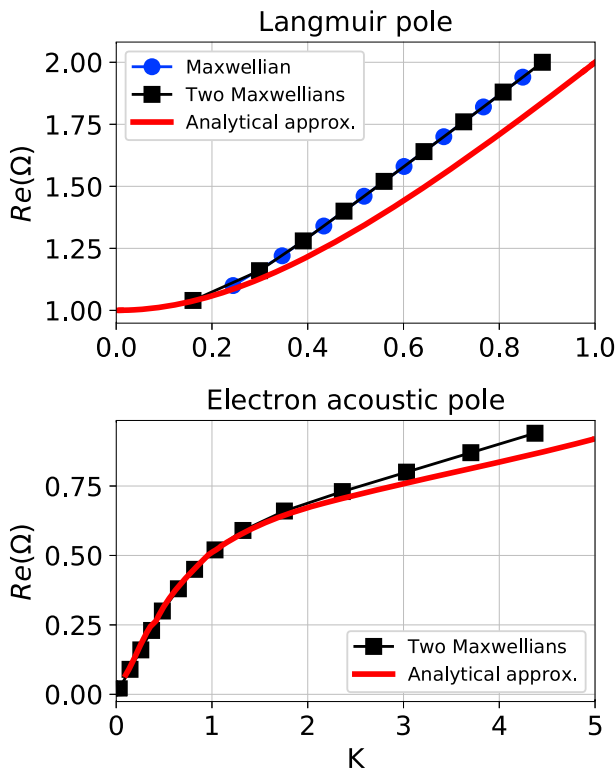


Figure 5. (top) Position of Langmuir pole for the numerical computation in the case of a Maxwellian evdf (blue circles) and a sum of two Maxwellian evdf (black squares, using $\mu = 100, \tau = 1$), together with the long-wavelength analytical approximation from the Langmuir dispersion relation equation (19) (red line). (bottom) Position of the electron acoustic pole from the numerical computation in the case of a sum of two Maxwellian evdf (black squares, $\mu = 1, \tau = 100$), together with the analytical approximation of the electron acoustic dispersion relation equation (21) (red line).

3. Finally, to further validate our numerical method, we compare our simulations with the mutual impedance spectra computed analytically in Pottelette and Storey (1981) for a double-dipole probe immersed in a Maxwellian or a two-electron temperature plasma. These comparisons are done for the perpendicular arrangement of a double-dipole probe, using the same parameters. Although the numerical integration is limited near the plasma frequency, the resulting spectra, shown in Figure 7, are identical to those reported in Figure 9 in Pottelette and Storey (1981). In particular, a local minimum is observed for the two cases near $\Omega = 1.30$. Note that the analytic dipole approximation is valid in the limit of (i) an emitter-receiver distance l much larger than the emitter-emitter and receiver-receiver distances d and (ii) an emitter-receiver distance much larger than the hot and cold Debye lengths: $l \gg d$ and $l \gg \lambda_{D,c}, \lambda_{D,h}$. For interplanetary spacecrafts, such as Rosetta, BepiColombo, and JUICE, the active electric antennas do not satisfied the configurations (i) and (ii). It is therefore necessary to develop a method that enables to take into account the mutual impedance experiments in interplanetary plasmas.

4. Application to Mutual Impedance Experiments

In this section, we make use of the plasma dielectric computed numerically as shown in the above section for different electron velocity distributions to build up synthetic spectra expected from mutual impedance experiments. We focus on mutual impedance spectra in a two-electron temperature plasma and compare them to the Maxwellian and cold plasma cases.

4.1. Mutual Impedance Spectra for Different Thermal Electron Populations

To better understand the influence of a evdf on mutual impedance measurements, in particular the influence of a hot electron population, it is worth comparing the theoretical spectra expected for a quadrupolar probe embedded in a cold, Maxwellian, or a sum of two Maxwellian plasma. To this purpose, we consider a quadrupolar probe with the geometry shown in Figure 3 and

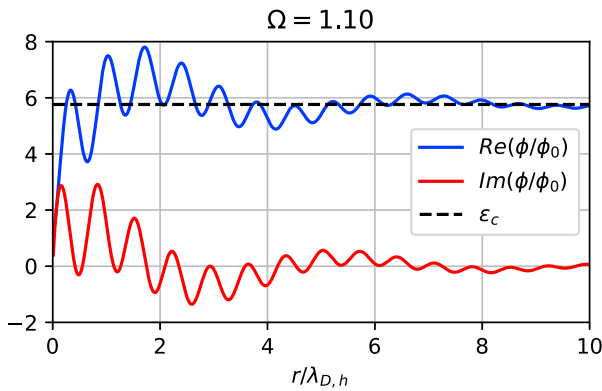


Figure 6. Real and imaginary parts of the electric potential ϕ/ϕ_0 (blue and red lines, respectively) radiated at frequency $\Omega=1.10$ in a two-electron temperature plasma $\mu=0.11$ and $\tau=100$, together with ϵ_c the asymptotic analytical limit of $\text{Re}(\phi/\phi_0)$ (dashed line).

show the associated mutual impedance spectra for different electron velocity distribution functions in Figure 8.

The mutual impedance resonance is expected at the plasma frequency for a cold plasma (blue curve), and close to the plasma frequency (depending on the emitter-receiver distance) for a single-temperature electron plasma (green curve). The behavior of the mutual impedance spectra above the plasma frequency is dominated by the influence of the less damped electrostatic mode that propagates in a Maxwellian plasma: the Langmuir waves. Those waves propagate at frequencies $\omega > \omega_p$ and are at the origin of destructive interferences on the receiving dipole that appear as local minima in the spectrum.

In a two-electron temperature plasma (orange and red curves), a second resonance appears at frequencies $\omega < \omega_p$, more specifically close to the cold plasma frequency $\omega_{p,c}$ (vertical black dotted line in both cases). It is associated to the propagation of another electrostatic mode that can propagate in two-electron temperature plasmas: the electron acoustic waves. This behavior has important consequences on the interpretation of mutual impedance experiments in collisionless plasmas. It implies that mutual impedance measurements in a plasma containing suprathermal electrons may be partially blind to the *total* plasma density but still provide a measure of the *cold* plasma density instead.

4.2. Mutual Impedance Spectra in a Two-Electron Temperature Plasma

The instrumental response of mutual impedance experiments in a two-electron temperature plasma strongly depends on the temperature and density ratios. To quantify it, the amplitude and phase of the mutual impedance spectra are computed in Figures 9 and 10, respectively, using the same geometric configuration as above, for different hot-to-cold temperature τ and density μ ratios, keeping the hot Debye length fixed $\lambda_{D,h}=0.10$ m. The temperature ratio increases from left to right, while the density of the cold population increases from bottom to top.

When the density of the hot electron component is much smaller than the cold component, the mutual impedance spectra show a clear, single maximum close to the plasma frequency (Figure 9, first row) associated to a phase rotation of 180° (Figure 10, first row). This is similar to what would be expected for a single Maxwellian plasma, where the influence of the hot population is seen in the amplitude and phase of the mutual impedance spectra at frequencies above the plasma frequency, through the thermal correction of the modified Langmuir waves (equation (20)). This thermal correction depends on the total electron pressure and is therefore strongly dominated by the hot electron component.

When the density of the hot electron component is of the order of the cold component (second to fourth rows, for instance $\mu=1$ and 2.33), a second resonance, associated to the existence of the electron acoustic mode, arises below the plasma frequency, at a frequency close to the cold plasma frequency (black vertical lines). The phase of the mutual impedance spectra is characterized by large rotations around the cold plasma frequency, up to several times 360° , as shown in Figure 10, second and third rows (in other words, the total phase shift is a multiple of 2π when crossing the cold plasma frequency). The phase shift increases with τ , while it decreases with N_h above a certain value. Note that a cutoff appears at the frequency corresponding to the frequency of the electron acoustic wave adapted to the receiving antenna (red vertical dotted lines).

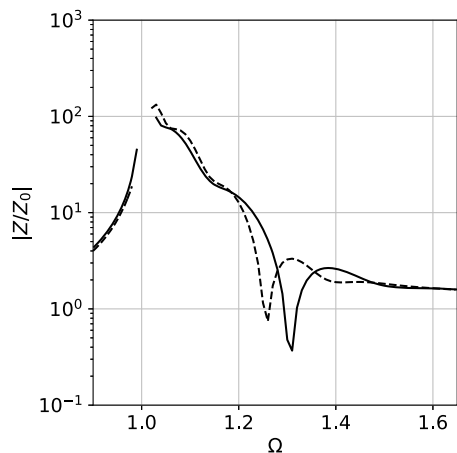


Figure 7. Normalized response, expressed in logarithmic scale as $20 \log_{10} (|Z(\Omega)/Z_0|)$ for the Maxwellian case with $\lambda_D=0.01$ m in black line on the double-dipole considered by Pottelette and Storey (1981) and for a sum of two Maxwellian evdf with $\mu=0.01$, $\tau=100$ and $\lambda_{D,h}=0.70$ m in black dashed line.

Figure 2.5 in Gary (1993) summarizes the domain of existence of electron acoustic waves in the (τ, μ) parameter plane. In particular, it shows that (i) the electron acoustic mode merges with the Langmuir mode for large cold electron ratio and (ii) the electron acoustic mode is strongly damped when the temperature ratio is not large enough, or for a too small cold electron ratio.

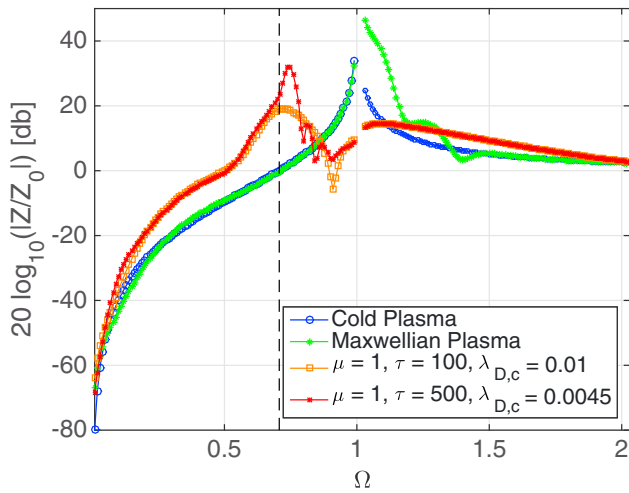


Figure 8. Normalized responses in power on the idealized mutual impedance probe (Figure 3) for different parameters μ and τ : cold electrons (blue), Maxwellian electrons (green), and a sum of two Maxwellian electrons configurations: $\mu = 1$, $\tau = 100$ (orange) and $\mu = 1$, $\tau = 500$ (red).

The mutual impedance spectra in Figures 9 and 10 are shown in the same (τ, μ) parameter plane to enable a direct comparison and interpretation: the resonance close to the cold plasma frequency is only observed in the domain of existence of the electron acoustic mode. In particular, it explains why no such low frequency resonance is observed for $\tau = 10$ (panels in the first column) or for $\mu = 0.11$ (panels in the first line).

5. Discussion and Conclusion

This study illustrates the influence of the electron velocity distribution function, in particular when considering cold, Maxwellian or a two-temperature electron plasma, on the instrumental response of mutual impedance experiments.

For that, the electrostatic potential radiated by a pulsating charge, written as an integral, is computed using a numerical integration on a sum of Maxwellian plasmas. To properly account for the weakly damped poles of the dielectric function located close to the path of integration, a method of grid refinement is proposed. The mutual impedance has been then computed on a probe made from two conducting spheres and two potential sensors. We have compared and validated the computation in the Maxwellian case with Beghin

(1995), which used a series expansion of the radiated potential, to support the computation in a sum of Maxwellian evdf.

In this work, we have assumed each emitter to be a point charge. We hereafter show that this hypothesis enables to tackle more complex geometries, and in particular, finite-size emitters.

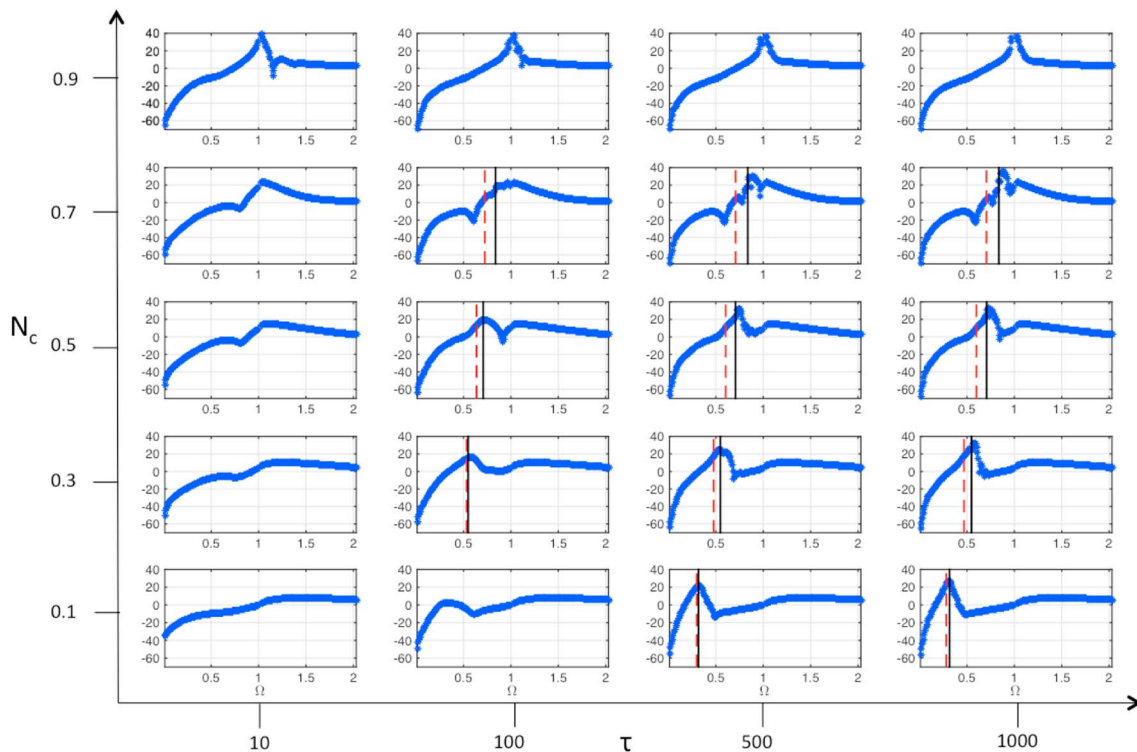


Figure 9. Amplitude of the normalized mutual impedance spectra, expressed in logarithmic scale as $20 \log_{10} (|Z(\Omega)/Z_0|)$, based on the probe configuration shown in Figure 3 for different temperature ratios $\tau = 10, 100, 500$, and 1000 , from left to right, and cold electron density ratios $N_c = 0.1, 0.3, 0.5, 0.7$, and 0.9 , from bottom to top. The hot Debye length is fixed $\lambda_{D,h} = 10$ cm. The red vertical dotted lines show the position of the electron acoustic pole, adapted to the receiving antenna, computed with the analytical dispersion relation equation (23). The black vertical lines show the cold plasma frequency $\omega_{p,c}$.

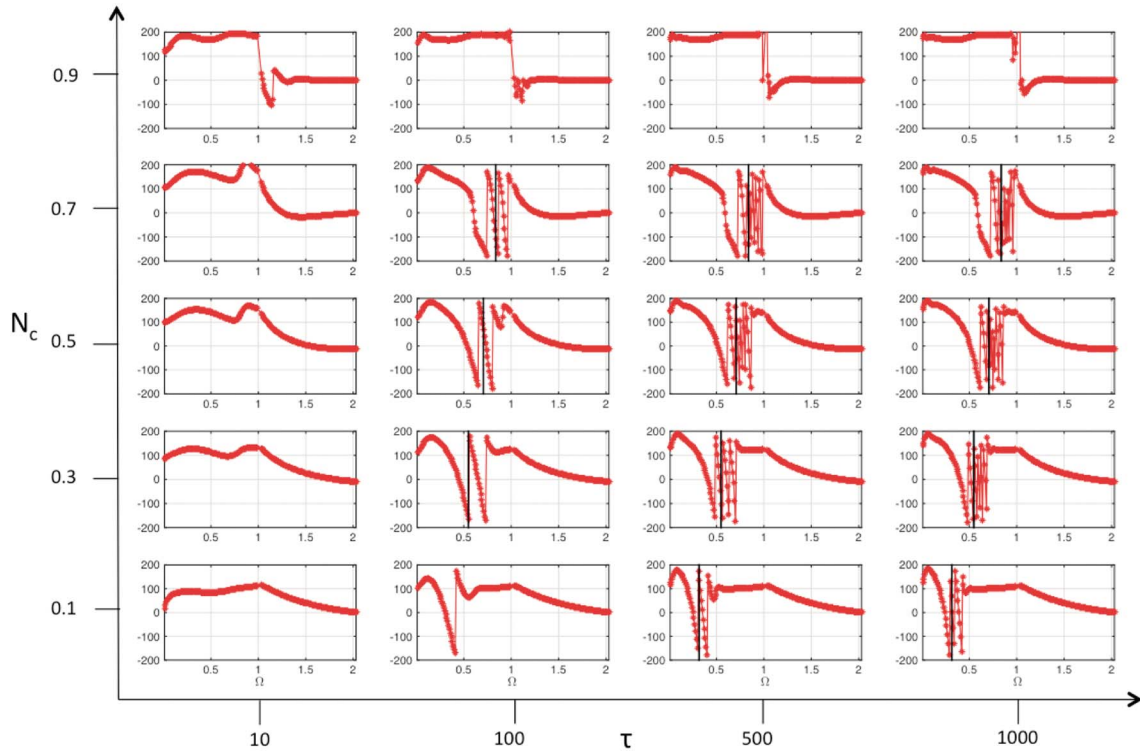


Figure 10. Phase in degree of the normalized mutual impedance spectra, corresponding to the amplitudes shown in Figure 9.

5.1. Influence of the Finite Probe Size on the Radiated Potential

Instead of a point source pulsating charge, if we consider the tip of an emitter as a sphere of radius a , the potential rewrites (Chasseriaux et al., 1972):

$$\frac{\phi_a}{\phi_0}(\Omega, R) = \frac{2R}{\pi} \int_0^\infty \frac{\sin(KR) \sin(Ka/\lambda_D)}{KR \frac{Ka/\lambda_D}{\epsilon_j(K, \Omega)}} dk \quad (24)$$

The influence of the added term $\sin(Ka/\lambda_D)/(Ka/\lambda_D)$ is significant when the ratio $a/\lambda_D > 1$. The Debye length being much larger than the size of emitters in typical interplanetary plasmas, the radiated potential ϕ_a/ϕ_0 is

of the order of ϕ/ϕ_0 . We have also compared the radiated potential emitted by a finite-size spherical emitter of radius a , using both (i) the analytic expression ϕ_a/ϕ_0 (equation (24)) and (ii) the potential computed by the classical Discrete Surface Charge Distribution (DSCD) method (Béghin & Kolesnikova, 1998), using a sum of point charges located on a sphere of radius a , each of which emits a point source potential ϕ/ϕ_0 . The results are shown in Figure 11: the DSCD method, which uses a sum of point charges, enables to reproduce the signal emitted by a finite-size source. It is therefore possible to extend the computation of the mutual impedance by taking into account a non punctual probe geometry, and/or the spacecraft itself to allow to measure the interaction with the spacecraft body (Geiswiller et al., 2001).

5.2. Practical Implications on Mutual Impedance Experiments Operated in Two-Electron Temperature Plasmas

This work has important practical implication regarding the interpretation of mutual impedance experiments data in a two-electron temperature plasma.

In the case of a two-electron temperature plasma, we have shown that two resonances can be found. First, a resonance located close to the total plasma frequency, as in the case of a single-electron temperature plasma. Second, another resonance appears close to the cold plasma frequency when the

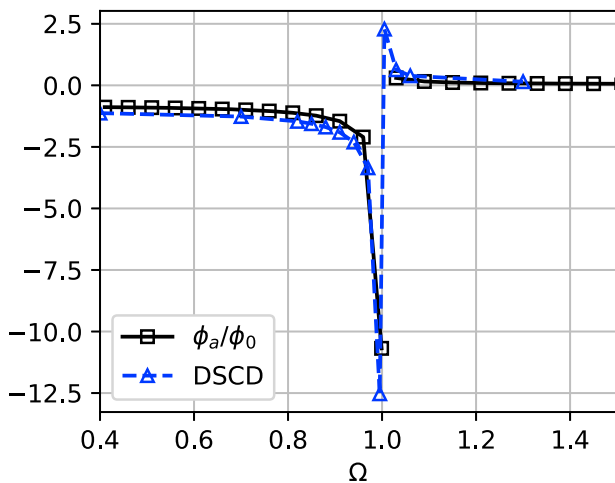


Figure 11. Amplitude of the radiated electric potential spectrum, expressed in logarithmic scale as $20 \log_{10}(|\phi/\phi_0(\Omega, a/\lambda_D)|)$, for $a = 0.03$ m and $\lambda_D = 0.3$ m, computed by equation (24) (squared black line) and by the Discrete Surface Charge Distribution (blue line).

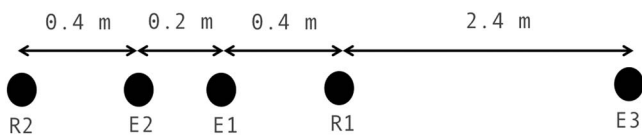


Figure 12. RPC-MIP in phase SDL operational mode.

temperature ratio is large enough (about 10 to 50, depending on the density ratio) and the hot electron population large enough (typically above 20%). The position of the resonance at the total plasma frequency can therefore be used to estimate the total electron density, as in a single-electron temperature plasma.

In a Maxwellian plasma, the electron temperature can be derived from a destructive interference pattern, located at frequencies larger than the plasma frequency and appearing as local minima in the spectrum. This interference pattern is associated to the thermal correction in the Langmuir waves dispersion relation (section 2.4). This method, detailed, for instance, in Trotignon et al. (2007), can only be applied when the Debye length is much smaller than the emitter-receiver distance ratio (typically an order of magnitude below). In a two-electron temperature plasma, a similar approach, based on a destructive interference pattern, can hardly be used. Indeed, the thermal correction in the (modified) Langmuir waves dispersion relation for a two-electron temperature plasma depends on the hot electron temperature. Therefore, a similar approach would be limited to cases where the hot Debye length is much smaller than the emitter-receiver distance ratio, which is very unlikely to happen in typical interplanetary plasmas for standard instrumentation. This implies that a direct measurement of the core electron temperature, based on these local minima, is not possible in a two-electron temperature plasma. Instead, a direct comparison of the shape of mutual impedance spectra is required (section 5.3).

Note that for a large parameter range, the resonance at the total plasma frequency may be flattened, while the main resonance in the mutual impedance spectra may be located close to the cold electron plasma frequency instead. In that case, there could be a risk of misinterpreting this single resonance with the well-known resonance at the total plasma frequency, which would result in a systematic error in plasma density measurements. In such a case, the behavior of the phase of the mutual impedance spectra can be necessary to identify the nature of the resonance and therefore enable a careful interpretation of mutual impedance spectra in the case of a two-electron temperature plasma to extract the plasma density.

Such behaviors strongly depend on the geometric configuration of the quadrupolar antenna, that is, on the relative distances between emitters and receivers. The choice of the geometry of quadrupolar mutual impedance probes is therefore crucial when operated in collisionless plasmas. The quadrupolar antenna configuration used in this study and shown in Figure 3 is therefore not optimal to distinguish between hot and cold plasma parameters. In some other spatial configurations, both resonances at the plasma frequency and at the cold plasma frequency are clearly identified, which enables to constrain the cold-to-hot density and temperature ratios. Below, we discuss such a more optimal configuration, used by the MIP instrument on board Rosetta, and we illustrate how we can distinguish between hot and cold plasma parameters.

5.3. Mutual Impedance Spectra Observed by Rosetta

The European Space Agency's Rosetta spacecraft has followed during more than 2 years the comet 67P/Churyumov-Gerasimenko from Summer 2014 to the end of September 2016 (Glassmeier et al., 2007). The mutual impedance probe MIP (Trotignon et al., 2007) on board Rosetta has measured the total electron density of the coma. The MIP antenna is a 1 m long bar with two receiving and two transmitting electrodes immersed in the cometary plasma. The emission frequencies range between 28 kHz and 3.5 MHz, where the plasma frequency is expected to be located. The cometary plasma can be approximated as unmagnetized in the MIP frequency range of operation, because the typical electron cyclotron frequency is orders of magnitude smaller than the typical plasma frequency. The assumptions made in this study therefore hold in a cometary plasma.

MIP-acquired responses in the so-called "phase SDL operational mode" are well reproduced by the ideal configuration presented in Figure 12 where point emitters E_1 and E_2 operate in phase with respective charge, normalized by the charge q_2 , $Q_1 = 0.75$ and $Q_2 = 1$, whereas point emitter E_3 which can be understood as the spacecraft electrostatic influence pulses with a normalized charge $Q_3 = -1.75$. Note that a modeling taking into account the probe geometry and the entire spacecraft is currently under development. During part of the Rosetta mission, two well-defined resonances have been observed in the mutual impedance spectra measured by MIP, consistent with what is expected in a two-electron temperature plasma. An example of such MIP spectrum is given in Figure 13 (black lines with asterisks). Note that (i) there is a known instrumental interference around 266 kHz (red shaded part of the spectrum) and (ii) spacecraft charging effects need to be taken into account at low frequencies (grey shaded part of the spectrum); future works will be dedicated to this task.

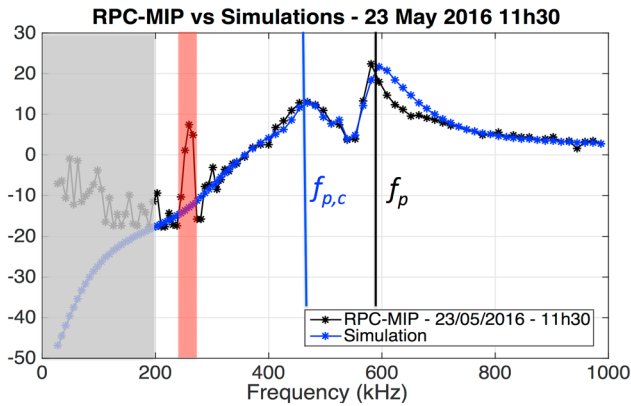


Figure 13. Amplitude of the mutual impedance spectra observed by MIP on board Rosetta on 23 May 2016 at 11h30 (black line with asterisks) and amplitude of a synthetic mutual impedance spectra computed in a two-electron temperature plasma (blue line with asterisks) corresponding to $N_h = 0.36$, $\tau = 103$, and $\lambda_{D,h} = 0.46$ m. In both cases the amplitude of the normalized mutual impedance spectra are expressed in logarithmic scale as $20 \log_{10} (|Z(\Omega)/Z_0|)$. The part in grey is not modeled, and the known interferences are in the red part.

The rest of the spectrum, above 300 kHz, shows two well-defined resonances, consistent with what is expected in a two-electron temperature plasma. To distinguish between the hot and cold plasma populations, we have computed a best fit of the observed MIP spectra with simulated mutual impedance spectra, computed for the corresponding geometry, shown in blue line with asterisks. The best fit, computed in the density and temperature ratios parameter space, is found for $N_h = 0.36$, $\tau = 103$, and $\lambda_{D,h} = 0.46$ m. With a plasma frequency $f_p \approx 600$ kHz, the density and the temperature of the two-electron populations can be derived. For this case, with the sensitivity of the comparison method, $n_h = 1500 \pm 150 \text{ cm}^{-3}$, $n_c \approx 2730 \pm 150 \text{ cm}^{-3}$, $T_h = 6 \pm 1.5 \text{ eV}$, and $T_c = 0.06 \pm 0.01 \text{ eV}$. The derived temperatures are consistent with the typical temperatures of warm and cold cometary electrons measured with the Langmuir Probe during the Rosetta mission (Eriksson et al., 2017).

6. Conclusions

We have shown that even a small proportion of suprathermal electrons can strongly modify different characteristic observational features from mutual impedance experiments, especially the evaluation of the electron temperature and in some cases the identification of the plasma frequency from which the plasma density is derived.

In the near future, we are confident the work described in this paper will allow to better interpret Rosetta RPC-MIP data in cases where the cometary plasma is characterized by a mix of cold and warm electrons. We also expect that this work will enable to better constraint the observation of mutual impedance experiments dedicated to space plasma in future planetary exploration missions, such as the future mutual impedance experiments PWI-AM2P that will fly on board the MMO spacecraft of the BepiColombo mission to Mercury (Trotignon et al., 2006), and RPWI-MIME that will fly on board the JUICE spacecraft to Jupiter and its moons, in particular Ganymede.

Finally, since space plasma are seldom thermalized, suprathermal electrons are often observed with large tails in the velocity distribution, which is not well described with Maxwellian function. Future works will be dedicated to generalizing the numerical approach described in this paper to nonthermal electron distributions that include suprathermal tails in the velocity distribution such as kappa distributions, in order to extend the applicability of mutual impedance experiments to such plasmas.

Appendix A: Computation of the Integral (22)

This section explains in more details the computation of the integral on the radiated potential expression (15). With some conditions on the integral limits, the integral I1 (equation (22)) can be evaluated analytically while I3 can be negligible for both Maxwellian and a sum of two Maxwellian cases. These conditions give the initial discretization of the K-space and R-space for the computation of I2 using a classical numerical integration (section 3). As said in the section 3.1, a grid refinement is required for frequency ω close to the plasma frequency ω_p to capture the strong variation of $1/\epsilon_l$.

A1. Numerical Computation of I1

On one hand, for all Ω , when $K \rightarrow 0$, $\text{Im}(1/\epsilon_l)$ tends toward 0 and $\text{Re}(1/\epsilon_l)$ converges to the inverse of dielectric function associated to the cold plasma limit, given by $\epsilon_c = \frac{1}{1-\Omega^2}$. Figure A1 shows these limits for $\Omega = 0.9$ and 1.5.

On the other hand, for $K \cdot R \ll \pi$, $\sin(KR)/KR \approx 1$. Therefore, the integral I1 can be approximated by

$$\frac{2R}{\pi} \int_0^{k_{\min}} \frac{1}{\epsilon_l(\Omega, K)} \frac{\sin(KR)}{KR} dK \approx \frac{2R}{\pi} \frac{k_{\min}}{1-\Omega^2} \quad (\text{A1})$$

for $k_{\min} \ll \pi/r_{\max}$ where r_{\max} is the maximum considered distance in the computation of the oscillating charge. r_{\max} depends on the configuration of the probe and the Debye length. In our study, we have chosen $r_{\max} = 10^3$ allowing to compute a mutual impedance for Debye length of the order of centimeter for the RPC-MIP

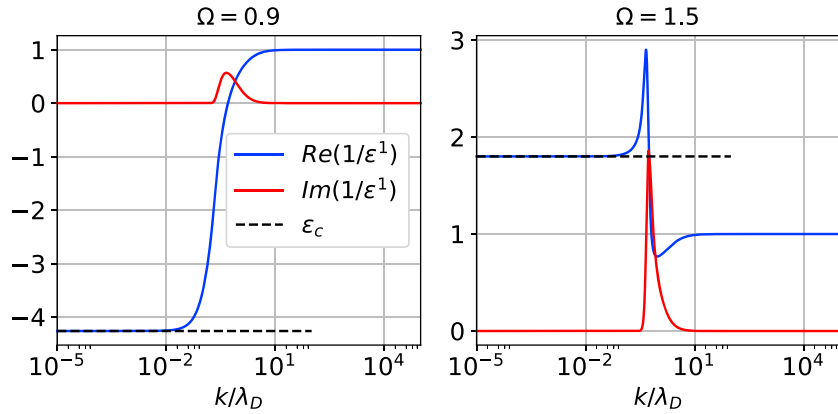


Figure A1. $\text{Re}(1/\epsilon_1^1)$ and $\text{Im}(1/\epsilon_1^1)$ for (left) $\Omega = 0.90$ and (right) $\Omega = 1.5$ for $K \in [10^{-5}, 10^5]$ in log scale, with the asymptotic limit $\epsilon_c = \frac{1}{1-\Omega^2}$ when $K \rightarrow 0$ (dashed line).

probe configuration. To satisfy equation (A1), k_{\min} is equal to 10^{-5} in the Maxwellian case and so that $k_{\min} \cdot r_{\max} = 10^{-2}$. For a sum of two Maxwellian evdf, we observe a numerical noise close to $k_{\min} = 10^{-5}$ due to the smallness of Y_c^2 for some parameters of μ and τ . k_{\min} is then equal to 10^{-4} . Note that the contribution (A1), added to the computation of the radiated potential ϕ/ϕ_0 , becomes nonnegligible at large distances from the oscillating charge.

A2. Numerical Computation of I3

Regarding the third term in equation (22), for K large enough ($K \gg K_i$ with K_i the normal modes of the plasma defined such that $\epsilon_i(K_i) = 0$), $\text{Re}(1/\epsilon_l) \rightarrow 1$ and $\text{Im}(1/\epsilon_l) \rightarrow 0$ (Figure A1). Therefore, integral I3 can be approximated by

$$\int_{k_{\max}}^{+\infty} \frac{\sin(KR)}{KR} dK \quad (\text{A2})$$

provided that $k_{\max} \gg K_i$.

First, for fixed K , integral (A2) increases when R tends toward 0. Assuming that the distance to the charge source r_{\min} is fixed, it is necessary to take a large k_{\max} to be able to neglect the integral (A2). In our study, we have chosen $k_{\max} = 10^5$ and $k_{\max} \cdot r_{\min} = 10^3$. Second, taking $k_{\min} = 10^{-5}$ and $k_{\max} = 10^5$ requires to use a logarithmic scale for K . With Δ_K the distance between two consecutive points in K -space, $\sin(KR)/KR$ cannot be computed properly for $\Delta_K \cdot R > \pi$. We have chosen to compute the integral only over K satisfying $\Delta_K \cdot R < \pi/6$ to avoid spurious numerical artifacts (Figure A2). For each distance R to the emitter, the maximum value of K that satisfies this condition, K_{\max}^{eff} , must be larger than the projections of the Langmuir pole on the integration path. As shown in Figure 5, the projection of this pole is smaller than $K = 1$ for Ω until $2f_p$. We have therefore

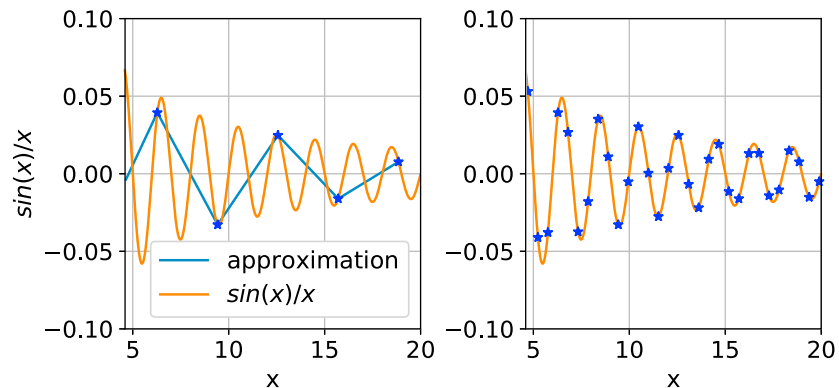


Figure A2. Comparison between $\sin(x)/x$ (orange line) and its discretization (blue asterisks) for the numerical method with (left) $\Delta_x = \pi$ and (right) $\Delta_x = \pi/6$.

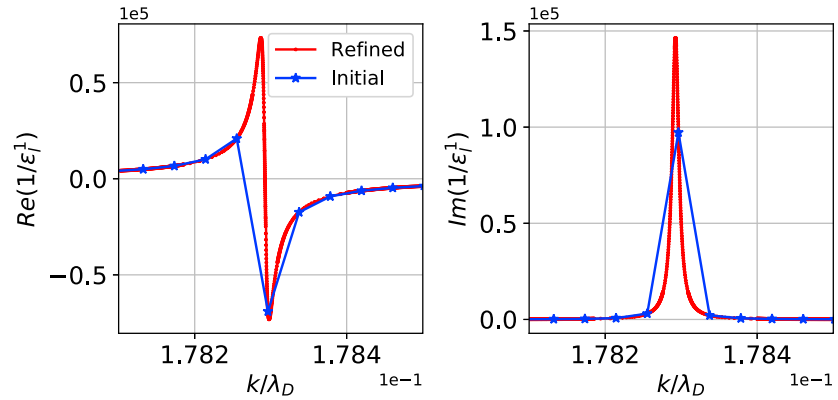


Figure A3. Comparison between an initial discretization (blue asterisk—10 points) on K-space (10^5 points in log scale on $[10^{-5}, 10^5]$) and refined (red point—933 points) discretization by the bisection method on the representation of (left) $\text{Re}(1/\epsilon_l^1)$ and (right) $\text{Im}(1/\epsilon_l^1)$, for $\Omega = 1.05$, $k_{\min} = 10^{-5}$ and $k_{\max} = 10^5$, with a zoom on the neighborhood of the Langmuir pole.

chosen $K_{\max}^{\text{eff}} > 2$. The smallest K_{\max}^{eff} is associated to the largest distance r_{\max} ; therefore, we need to take the number of points on K-space, N_K , high enough (here chosen to be 10^5) to satisfy $K_{\max}^{\text{eff}}(r_{\max}) > 2$ with $r_{\max} = 10^3$. For the sum of two Maxwellian evdf, we consider for large distances R that the electron acoustic pole is already damped. Using the Dirichlet integral, the higher $(2R/\pi)/3$, corresponding to the case $K_{\max}^{\text{eff}} = 2$ and $R = 10^3$, is on the order of 10^{-4} . The relative error of the computed $\phi/\phi_0(\Omega, 10^3)$, given by $|10^{-4}/\epsilon_c|$, is smaller than 10^{-2} for $\Omega > 0.05$ and on the order of 1 for $\Omega < 0.02$.

A3. Numerical Computation of I2

To evaluate I_2 , the dielectric function ϵ_l^m , given by equation (8), has been computed using the relation (13) between the plasma dispersion function Z and the Faddeeva function w , given by equation (14), implemented on the Faddeeva package (Johnson, 2012). This package uses the method of Poppe and Wijers (1990) and Zaghoul and Ali (2012) to compute the Faddeeva function. The dielectric and the sinc functions are calculated on an initial K-space discretization (10^5 points in log scale on $[10^{-5}, 10^5]$) constrained by the conditions imposed on I1 (Appendix A1) and I3 (Appendix A2). I_2 is computed with a classical numerical integration, using a trapezoidal rule (Press et al., 2007). As said in section 3.1, the discrete K-space needs to be refined in the close vicinity of the weakly damped pole. The first step of the grid refinement is finding the location of the projection on the real axis of the least damped pole K_l . To this purpose, we use a secant method (Press et al., 2007) to identify the zero of the real part of the dielectric function. The iterative method is initialized by the long-wavelength analytical approximation of the Langmuir wave vector K_L at the considered frequency using equation (19):

$$K_L = \sqrt{\frac{\Omega^2 - 1}{3}} \quad (\text{A3})$$

At convergence, this procedure enables to find a precise location of projection of K_l on the real axis, defined as k_{sec} , which can significantly differ from K_L at frequencies well above the plasma frequency.

The next step is refining the K-space to capture the strong variations of $1/\epsilon_l^m$. k_{sec} being an approximation of the maximum of $\text{Im}(1/\epsilon_l^m)$, we uniformly discretize values of $\text{Im}(1/\epsilon_l^m)$, called y_i until the approximated maximum. Using a bisection method (Press et al., 2007) on the function $f = g\left(\frac{1}{\epsilon_l^m}\right) - y_i$, with g the real or imaginary part, we find the corresponding values on K-space. For this method, the starting range $[a, b]$ on K-space must be satisfied (i) the opposite signs of $f(a)$ and $f(b)$ and (ii) the uniqueness of the zero of f . A second grid refinement step can be applied for practical reasons. An example of this new discretization is illustrated on Figure A3 for $\text{Re}(1/\epsilon_l^1)$ and $\text{Im}(1/\epsilon_l^1)$ at $\Omega = 1.05$, showing the initial mesh (blue asterisks) together with the refined mesh (red points).

For a sum of two Maxwellian evdf, the refinement method is essentially the same as described in the previous section, with two slight changes. (i) The starting point of the secant method, to approximate the location of the (modified) Langmuir pole, is now taken from the approximation of the zero of $\text{Re}(\epsilon_l^2)$, which is directly

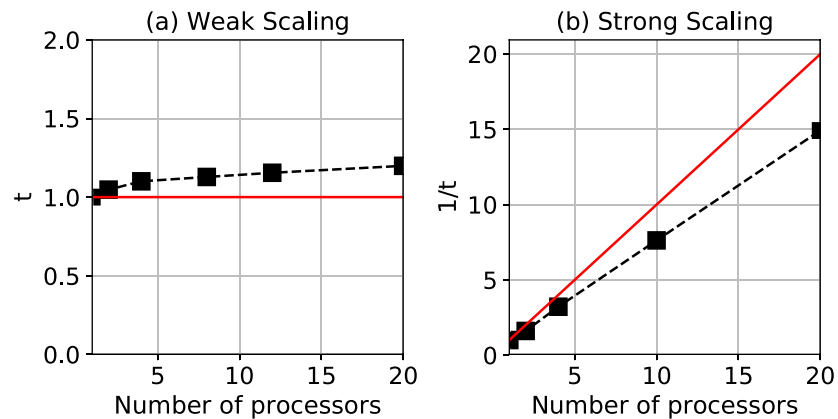


Figure A4. (a) Weak and (b) strong scaling (black dashed lines) for the parallelization of the computation of the radiated potential for a sum of two Maxwellian plasmas (section 2.2) compared with the optimal scaling (red lines).

found on an initial, not yet refined, grid. (ii) To ensure bijection in the considered K range, the bisection method is initialized far enough from the projection of the location of electron acoustic pole. For this paper, computations of the radiated potential on the Maxwellian case have been carried out for two hundred frequencies Ω in the range $[0.01, 0.99] \cup [1.03, 2]$, for $K \in [10^{-5}, 10^5]$ in log scale with 10,000 points, with a grid refinement of 3,000 points when $\Omega \in [1.03, 1.08]$, and for $R \in [10^{-2}, 10^3]$. In the range $\Omega \in [1, 1.02]$, the least damped pole K_1 is too close to the real axis to enable a proper discretization of $1/\epsilon_1^1$, limited by the numerical noise. Indeed, the step of the grid refinement is of the order of the precision of routines used in the code. For a sum of two Maxwellian evdf, it is possible also to compute the radiated potential for Ω smaller than 1.03 for a selected parameters μ and τ . The serial computation on a PC lasts about 750 s for 2,000 points on the R-space. The algorithm has been written in Fortran 90 with an interoperability with C++ for the Faddeeva package.

A4. Scalability of the Parallel Computing

While the computation of the radiated electric potential for a Maxwellian evdf depends only on the frequency of the oscillating point charge and the distance to this charge, the computation of the radiated electric potential for a multi-Maxwellian evdf also depends on the density and temperature ratios (resp. μ and τ). To efficiently compute it on the much larger four-parameter space in the case of two Maxwellian evdf, the algorithm has been parallelized with OpenMP, a multithreading tool. The outputs are parallelized as well; the ratio between sequential and parallelize regions is therefore very small. To analyze the performance of this parallelization, a weak scaling and a strong scaling have been calculated (Figure A4). The weak scaling shows the computation performance decrease associated to memory access. For instance, with 20 threads, the computation CPU time raises by 20%. The strong scaling gives the acceleration of the parallelization and the optimal number of processors. For 20 threads, the computation is 15 times higher than the sequential one. The algorithm have run on a maximum of 20 threads in the cluster of the région Centre, France, named Artemis (CaSciModOT project).

Acknowledgments

This work was supported by CNES and by ANR under the financial agreement ANR-15-CE31-0009-01. We acknowledge the financial support of label ESEP (Exploration Spatiale des Environnements Plantaires). The Rosetta RPC-MIP mutual impedance spectra are publicly available on the ESA Planetary Science Archive (PSA). The authors benefited from the use of the cluster Artemis (CaSciModOT) at the Centre de Calcul Scientifique en région Centre-Val de Loire (CCSC). Part of this work was inspired by discussions within International Team 336: “Plasma Surface Interactions with Airless Bodies in Space and the Laboratory” at the International Space Science Institute, Bern, Switzerland.

References

- Bahnens, A., Jespersen, M., Ungstrup, E., Pottelette, R., Malingre, M., Decreau, P. M. E., ... Pedersen, B. M. (1986). First VIKING results: High frequency waves (NASA STI/Recon Technical Report N, 87).
- Beghin, C. (1995). Series expansion of electrostatic potential radiated by a point source in isotropic Maxwellian plasma. *Radio Science*, 30, 307–322. <https://doi.org/10.1029/94RS03167>
- Beghin, C., & Debrie, R. (1972). Characteristics of the electric field far from and close to a radiating antenna around the lower hybrid resonance in the ionospheric plasma. *Journal of Plasma Physics*, 8, 287–310. <https://doi.org/10.1017/S0022377800007157>
- Beghin, C., Debrie, R., Berthelier, J. J., Roux, D., Galperin, I. I., Gladyshev, V. A., & Masevich, N. I. (1982). High resolution thermal plasma measurements aboard the Aureol 3 spacecraft. *Advances in Space Research*, 2, 61–66.
- Béghin, C., & Kolesnikova, E. (1998). Surface-charge distribution approach for modeling of quasi-static electric antennas in isotropic thermal plasma. *Radio Science*, 33, 503–516. <https://doi.org/10.1029/97RS03588>
- Buti, B., & Yu, M. Y. (1981). Langmuir solitons in a two-temperature plasma. *Journal of Plasma Physics*, 26, 309–316. <https://doi.org/10.1017/S0022377800010692>
- Chassériaux, J. M., Debrie, R. D. R., & Renard, C. R. C. (1972). Electron density and temperature measurements in the lower ionosphere as deduced from the warm plasma theory of the h.f. quadrupole probe †. *Journal of Plasma Physics*, 8, 231–253. <https://doi.org/10.1017/S0022377800007108>
- Décrou, P. M. E., Beghin, C., & Parrot, M. (1978). Electron density and temperature, as measured by the mutual impedance experiment on board GEOS-1. *Space Science Reviews*, 22, 581–595. <https://doi.org/10.1007/BF00223942>

- Eriksson, A. I., Engelhardt, I. A., André, M., Boström, R. I., Edberg, N., Karlsson, T., ... Norberg, C. (2017). Cold and warm electrons at comet 67P. *Astronomy and Astrophysics*, *605*, 30159. <https://doi.org/10.1051/0004-6361/201630159>
- Fried, B. D., & Conte, S. D. (1961). *The plasma dispersion function*. New York: Academic Press.
- Gary, S. P. (1993). *Theory of space plasma microinstabilities* (193 pp.). Cambridge, UK: Cambridge University Press.
- Geiswiler, J., Béghin, C., Kolesnikova, E., Lagoutte, D., Michau, J. L., & Trotignon, J. G. (2001). Rosetta spacecraft influence on the mutual impedance probe frequency response in the long Debye length mode. *Planetary and Space Science*, *49*, 633–644. [https://doi.org/10.1016/S0032-0633\(00\)00173-2](https://doi.org/10.1016/S0032-0633(00)00173-2)
- Glassmeier, K.-H., Boehnhardt, H., Koschny, D., Kürt, E., & Richter, I. (2007). The Rosetta mission: Flying towards the origin of the solar system. *Space Science Reviews*, *128*, 1–21. <https://doi.org/10.1007/s11214-006-9140-8>
- Grard, R. (1969). Coupling between two electric aerials in a warm plasma. *Alta Frequency*, *38*, 97–101.
- Grard, R. (1997). Influence of suprathermal electrons upon the transfer impedance of a quadrupolar probe in a plasma. *Radio Science*, *32*, 1091–1100. <https://doi.org/10.1029/97RS00254>
- Johnson, S. G. (2012). *Faddeeva package*. Retrieved from http://ab-initio.mit.edu/wiki/index.php/Faddeeva_Package
- Krall, N. A., & Trivelpiece, A. W. (1973). *Principles of plasma physics*. New York: McGraw-Hill Book Company.
- Nave, M., Bertrand, P., Feix, M., Rooy, B., & Storey, L. (1971). Problemes et modeles en theorie des sondes radiofrequences. *Journal de Physique Colloques*, *32(C5)*, C5b–189–C5b–191. <https://doi.org/10.1051/jphyscol:19715120>
- Odelstad, E., Eriksson, A. I., Edberg, N. J. T., Johansson, F., Vigren, E., André, M., ... Cupido, E. (2015). Evolution of the plasma environment of comet 67P from spacecraft potential measurements by the Rosetta Langmuir probe instrument. *Geophysical Research Letters*, *42*, 10,126–10,134. <https://doi.org/10.1002/2015GL066599>
- Pierrard, V., & Lazar, M. (2010). Kappa distributions: Theory and applications in space plasmas. *Solar Physics*, *267*, 153–174. <https://doi.org/10.1007/s11207-010-9640-2>
- Pilipp, W. G., Muehlhaeuser, K.-H., Miggenrieder, H., Montgomery, M. D., & Rosenbauer, H. (1987). Characteristics of electron velocity distribution functions in the solar wind derived from the HELIOS plasma experiment. *Journal of Geophysical Research*, *92*, 1075–1092. <https://doi.org/10.1029/JA092iA02p01075>
- Poppe, G. P. M., & Wijers, C. M. J. (1990). More efficient computation of the complex error function. *ACM Transactions on Mathematical Software*, *16*(1), 38–46. <https://doi.org/10.1145/77626.77629>
- Pottelette, R., Rooy, B., & Fiala, V. (1975). Theory of the mutual impedance of two small dipoles in a warm isotropic plasma. *Journal of Plasma Physics*, *14*, 209–243. <https://doi.org/10.1017/S0022377800009533>
- Pottelette, R., & Storey, L. R. O. (1981). Active and passive methods for the study of non-equilibrium plasmas using electrostatic waves. *Journal of Plasma Physics*, *25*, 323–350. <https://doi.org/10.1017/S0022377800023151>
- Press, W. H., Teukolsky, S. A., Vetterling, W. T., & Flannery, B. P. (2007). *Numerical recipes: The art of scientific computing*. New York: Cambridge University Press.
- Rooy, B., Feix, M. R., & Storey, L. R. O. (1972). Theory of a quadrupolar probe for a hot isotropic plasma. *Plasma Physics*, *14*, 275–300. <https://doi.org/10.1088/0032-1028/14/3/005>
- Storey, L. R. O. (1998). Mutual-impedance techniques for space plasma measurements. In *Measurement techniques in space plasmas—Fields, Geophysical Monograph Series* (Vol. 103, pp. 155). Washington DC: American Geophysical Union. <https://doi.org/10.1029/GM103p0155>
- Storey, L. R. O., Aubry, M. P., & Meyer, P. (1969). A quadrupole probe for the study of ionospheric plasma resonances. In J. O. Thomas & B. J. Landmark (Eds.), *Plasma waves in space and in the laboratory* (303 pp.). New York: American Elsevier.
- Trotignon, J. G., Béghin, C., Lagoutte, D., Michau, J. L., Matsumoto, H., Kojima, H., ... Pottelette, R. (2006). Active measurement of the thermal electron density and temperature on the Mercury Magnetospheric Orbiter of the BepiColombo mission. *Advances in Space Research*, *38*, 686–692. <https://doi.org/10.1016/j.asr.2006.03.031>
- Trotignon, J. G., Michau, J. L., Lagoutte, D., Chabassière, M., Chalumeau, G., Colin, F., ... Zamora, P. (2007). RPC-MIP: The mutual impedance probe of the Rosetta plasma consortium. *Space Science Reviews*, *128*, 713–728. <https://doi.org/10.1007/s11214-006-9005-1>
- Zaghloul, M. R., & Ali, A. N. (2012). Algorithm 916: Computing the Faddeyeva and Voigt functions. *ACM Transactions on Mathematical Software*, *38*(2), 15:1–15:22. <https://doi.org/10.1145/2049673.2049679>